REPORT DOCUMENTATION PAGE

Form Approved
OMB No. 0704-0188

1. REPORT DATE *(DD-MM-YYYY)*
03-11-2003

2. REPORT TYPE
REPRINT

3. DATES COVERED *(From - To)*

4. TITLE AND SUBTITLE
Methods for Improving Seismic Event Location Processing

5a. CONTRACT NUMBER
DTRA01-01-C-0085

5b. GRANT NUMBER

5c. PROGRAM ELEMENT NUMBER

6. AUTHOR(S)
C. H. Thurber, W. Du, H. Zhang and W. J. Lutter

5d. PROJECT NUMBER
DTRA

5e. TASK NUMBER
OT

5f. WORK UNIT NUMBER
A1

7. PERFORMING ORGANIZATION NAME(S) AND ADDRESS(ES)
University of Wisconsin-Madison
Department of Geology and Geophysics
1215 W. Dalton Street
Madison, WI 53706

8. PERFORMING ORGANIZATION REPORT

9. SPONSORING / MONITORING AGENCY NAME(S) AND ADDRESS(ES)
Air Force Research Laboratory
29 Randolph Road
Hanscom AFB MA 01731-3010

10. SPONSOR/MONITOR'S ACRONYM(S)
AFRL/VSBYE

11. SPONSOR/MONITOR'S REPORT NUMBER(S)
AFRL-VS-TR-2003-1603

12. DISTRIBUTION / AVAILABILITY STATEMENT
Approved for Public Release; Distribution Unlimited.

13. SUPPLEMENTARY NOTES
REPRINTED FROM: PROCEEDINGS OF THE 25TH SEISMIC RESEARCH REVIEW - NUCLEAR EXPLOSION MONITORING,'BUILDING THE KNOWLEDGE BASE', 23-25 September 2003, Tucson, AZ pp 342-351.

14. ABSTRACT
Our research program consists of four components, each involving some aspect of multiple-event analysis: (1) high-precision waveform cross-correlation (WCC) for arrival time estimation, (2) robust event clustering, (3) waveform decomposition and source wavelet deconvolution reshaping, (4) double-difference (DD) multiple-event locations and tomography. Our research focused initially on the development and testing of these seismic analysis methods using ''ground-truth'' (GT) datasets at different scales (local and regional), and is being followed by the application of these methods to a ''test bed'' regional-distance seismic dataset, including tests on real-time and simulated real-time data streams. Here we highlight some of the more significant project achievements from components 1, 2 and 4.

15. SUBJECT TERMS
Seismic events Seismic deconvolution Seismic tomography Seismic location
Double-difference method Robust event cluttering Waveform cross-correlation

16. SECURITY CLASSIFICATION OF:			17. LIMITATION OF ABSTRACT	18. NUMBER OF PAGES	19a. NAME OF RESPONSIBLE PERSON
a. REPORT	b. ABSTRACT	c. THIS PAGE			Robert Raistrick
UNCLAS	UNCLAS	UNCLAS	SAR	11	19b. TELEPHONE NUMBER *(include area code)* 781 377-3726

ANNUAL SCIENTIFIC REPORT

METHODS FOR IMPROVING SEISMIC EVENT LOCATION PROCESSING

Clifford H. Thurber, Wen-xuan Du, Haijiang Zhang, and William J. Lutter

Department of Geology and Geophysics, University of Wisconsin-Madison

Sponsored by Air Force Research Laboratory

Contract No. DTRA01-01-C-0085

ABSTRACT

Our research program consists of four components, each involving some aspect of multiple-event analysis: (1) high-precision waveform cross-correlation (WCC) for arrival time estimation, (2) robust event clustering, (3) waveform decomposition and source wavelet deconvolution reshaping, (4) double-difference (DD) multiple-event location and tomography. Our research focused initially on the development and testing of these seismic analysis methods using "ground-truth" (GT) datasets at different scales (local and regional), and is being followed by the application of these methods to a "test-bed" regional-distance seismic dataset, including tests on real-time and simulated real-time data streams. Here we highlight some of the more significant project achievements from components 1, 2, and 4.

(1) Differential arrival times for pairs of seismic events observed at the same station are often calculated by WCC techniques. Researchers often choose the differential times to use based on the associated cross-correlation (CC) values exceeding a specified threshold. When two similar time series are corrupted by correlated noise, the time delay estimate calculated with the WCC technique may not be reliable. Thus the selection of a threshold value is important. If it is set too high, then only a limited number of very accurate differential time data are available to constrain the relative positions of earthquakes. If the threshold value is set too low, then many unreliable differential time estimates are used and they will negatively affect the final relocation results. The bispectrum method can suppress the correlated Gaussian noise sources in two similar time series and be used to obtain the relative time delay between them. We compute time delay estimates between the waveform pairs with the bispectrum method and use them to verify the WCC-determined one. This technique can provide quality control over the selected time delay estimates and potentially provide more differential travel time data for close events pairs, by verifying the reliability of differential times that might not meet the threshold criterion.

(2) We have tested a two-step event location technique with a California GT data set. In step 1, event locations are estimated via WCC of Hilbert-envelope waveforms. The Step 1 procedure accurately located the epicenters within 20 km (approximately 1 bin) of the NCSN catalog location for 16 of the 20 test events. However, depth estimates were poorly constrained. The Step 2 refinement based on WCC of the high-frequency P arrivals followed by DD relocation improved both epicenter and depth estimates. This two-step procedure offers advantages over conventional location techniques including a Step 1 event location not dependent on the accuracy of catalog picks and a Step 2 improvement in location accuracy using the high-accuracy DD technique.

(3) We have developed the new method of DD tomography. The inversion code tomoDD takes the double-difference location method (hypoDD) a step further to solve for 3D velocity structure simultaneously with hypocenter locations using both catalog picks and differential arrival times (WCC and catalog). Compared to conventional tomography, the result is a sharpening of the seismicity distribution equal in quality to hypoDD plus a sharpening of the velocity image due to removal of the majority of the location scatter. We have developed local- and regional-scale versions of tomoDD, and have applied each to synthetic and real datasets.

OBJECTIVE

Our research program consists of four components, each involving some aspect of multiple-event analysis: (1) high-precision waveform cross-correlation (WCC) for arrival time estimation, (2) robust event clustering, (3) waveform decomposition and source wavelet deconvolution reshaping, (4) double-difference (DD) multiple-event location and tomography. Our research focused initially on the development and testing of these seismic analysis methods using "ground-truth" (GT) datasets at different scales (local and regional), and is being followed by the application of these methods to a "test-bed" regional-distance seismic dataset, including tests on real-time and simulated real-time data streams. Here we highlight some of the more significant project achievements from components 1, 2, and 4.

RESEARCH ACCOMPLISHED

Bispectrum analysis

Differential arrival times for pairs of seismic events observed at the same station are often calculated by WCC techniques. These differential times (or adjusted picks derived from them) can be used to improve dramatically the earthquake relocation results (Got et al., 1994; Dodge et al., 1995; Shearer, 1997; Rubin et al., 1999; Waldhauser and Ellsworth, 2000; Schaff et al., 2002). Researchers often choose the differential times to use based on the associated CC values exceeding a specified threshold. For example, Schaff et al. (2002) only selected those time delays with CC values larger than 0.7 and mean coherences above 0.7. The selection of an "optimum" threshold value is important but difficult. If it is set too high, then only a limited number of very accurate differential time data are available to constrain the relative positions of earthquakes. On the other hand, if the threshold value is set too low, then many unreliable differential time estimates are used and will negatively affect the final relocation results. Also the time delay estimate calculated with the CC technique may not be reliable when the noise sources in the two time series are correlated.

The WCC approach and its variants work in the second-order spectral domain. When the underlying signal inside two similar time series can be regarded as a non-Gaussian process and the noise sources as zero-mean Gaussian processes, the similarities between the two time series can be better compared in the third-order or bispectrum domain (Nikias and Raghuveer, 1987; Nikias and Pan, 1988; Yung and Ikelle, 1997). This bispectrum method takes advantage of the fact that for Gaussian processes only all spectra of order higher than two are identically zero. Thus the effect of correlated Gaussian noise is completely suppressed when we compare the two time series in the bispectrum domain, while it may make WCC techniques fail to work well. Noise at a station for different events can be expected to be partially correlated due to a combination of constant predominant noise sources with time-varying amplitude (microseisms, wind or cultural noise) and site response effects. Cycle skips are another potential WCC pitfall that bispectrum analysis may help detect.

Figure 1 demonstrates the application of the CC and bispectrum methods to the waveforms of two closely spaced M2.5 New Zealand earthquakes. The waveforms for these events recorded at nearby stations are highly similar, but the signal to noise ratios (SNRs) for the records at station MOW (epicentral distance of 93 km) are noticeably lower (Figs. 1A and 1B). The two bispectrum-correlation series (Figs. 1E and 1F) peak at lag 6 and 7 respectively, whereas the two CC series (Figs. 1C and 1D) reach maxima at lags very different from each other and also from the two bispectrum-correlation series. Careful examination reveals that the two CC series reach local maxima at lag 7. They fail to become global maxima there, however, apparently due to the contamination of correlated noise. Figures 1G and 1H plot the stacked signals for both raw and band-pass filtered waveforms. In both cases the lower trace (the stacked signal obtained by shifting the waveform of the first event with bispectrum-determined lags) has a larger root-mean-square (RMS) amplitude than the upper trace, which is obtained after shifting the waveform of the first event with the CC-determined lags. The above example corroborates the findings of Nikias and Pan (1988) and Yung and Ikelle (1997) that the bispectrum method works better than CC techniques in getting relative time delay between two similar signals contaminated by correlated noise.

In our approach, we compute two more time delay estimates between the waveform pairs with the bispectrum method (the raw data and band-pass filtered data) and use them to verify the WCC-determined one using the band-pass filtered data. This technique can provide quality control over the selected time delay estimates and potentially provide more differential travel time data for close events pairs, by verifying the reliability of differential times that might not meet the threshold criterion.

The process of time delay calculation and bispectrum verification can be briefly described as follows. For the k-th mutual station that provides waveforms for two earthquakes i and j, we rely on the catalog phase (P or S) picks to

form the data windows used for time delay calculations. Then using the band-pass filtered waveforms, we calculate both the CC value CC_{ij}^{k} and the relative time delay in lag number $\Delta_{ij}^{k(cc)}$ for the event pair. If the value of CC_{ij}^{k} is larger than a threshold CC^{sub}, we also perform sub-sample time delay calculation to get $\Delta_{ij}^{k(sub)}$ by a weighted linear fitting of the cross spectrum phase (Poupinet et al., 1984). After we make the CC calculations for all the mutual stations between events *i* and *j*, we can obtain the maximum CC value CC_{ij}^{max} for the event pair. If CC_{ij}^{max} is larger than a second threshold CC^{bs}, we will perform bispectrum time delay estimation for each mutual station of the event pair. We obtain two estimates of time delay in lag number, i.e. $\Delta_{ij}^{k(bs1)}$ using the band-pass filtered waveforms and $\Delta_{ij}^{k(bs2)}$ with the raw waveforms. Thus depending on the extent of waveform similarity for an event pair, which is measured by the size of CC_{ij}^{max}, four possible time delay estimations are carried out at a mutual station for either P or S waves.

Besides the aforementioned threshold value that researchers often use to select time delay estimates, which we term CC^{lim1}, three other parameters CC^{lim2}, CC^{lim3} and Δ^{lim} control the bispectrum verification process. Generally $CC^{lim2} \geq CC^{lim1} \geq CC^{lim3}$. After we make the CC calculations across all the mutual stations of an event pair, we compare the maximum CC value CC_{ij}^{max} with CC^{lim2}. If CC_{ij}^{max} is larger than CC^{lim2}, we will verify the CC time delay estimates for those stations with CC_{ij}^{k} larger than CC^{lim3}. A CC time delay estimate $\Delta_{ij}^{k(cc)}$ is trusted (or passes the verification) if its differences from both $\Delta_{ij}^{k(bs1)}$ and $\Delta_{ij}^{k(bs2)}$, the ones determined with the bispectrum method, do not exceed the tolerance limit Δ^{lim}. In other words, for an event pair with high CC_{ij}^{max} value we will select the CC time delay estimates as long as they pass the bispectrum verification, even though the CC values associated with some of them are smaller than CC^{lim1} and would not be used under the threshold criterion often adopted by other researchers. If $CC^{lim1} \leq CCij^{max} < CC^{lim2}$, we will make the verifications only for those stations with CC_{ij}^{k} larger than CC^{lim1}. If CC_{ij}^{max} falls below CC^{lim1}, the CC time delays for the event pair are simply discarded.

As an example, we apply this technique to obtain bispectrum-verified WCC differential times for a set of New Zealand earthquakes, and relocate 521 of the events using the DD algorithm hypoDD (Waldhauser and Ellsworth, 2000). We find that the bispectrum-verified time delays provide more clustered earthquake relocation results with lower arrival time residuals compared to the threshold criterion. Figure 2 shows the relocation results for a subregion near Lake Wairarapa, New Zealand.

Generally for an earthquake, fewer S arrivals are available in the phase catalog than P arrivals because they are more difficult to select. We can obtain additional bispectrum-verified S differential times for those waveforms lacking catalog S picks, using the predicted S arrivals either from a velocity model (Shearer, 1997) or from the S-P time of a nearby event. Our work demonstrates that relocation results can be further improved with these additional time constraints.

Hierarchical clustering and location

We have implemented and tested a two-step location technique that offers several advantages over conventional techniques due to its use of WCC and DD location methods. Step 1 event location is based solely on high-quality GT event waveforms without use of catalog picks. Step 2 location estimates offer the same improvement in location accuracy as documented by the use of high-resolution DD techniques over standard techniques (Waldhauser and Ellsworth, 2000). We evaluated the technique using 640 events from N. California (magnitude range 4.3-5.3) using a 6°x 6° study region and 7 master stations from the UC Berkeley NCSN array (Fig. 3). In step 1, event locations are estimated via CC of Hilbert-envelope waveforms. A test event is cross-correlated against a suite of reference events binned by latitude, longitude, and depth. The step 1 location derived from the CC global maximum is then used as a starting location in the step 2 refinement using the DD relocation method (hypoDD).

All events were initially binned using the catalog locations into 0.1° latitude and longitude bins and 1.5 km depth bins. We selected the highest magnitude event per bin as a reference event. We assembled a suite of test events by selecting the second highest magnitude event from each multiple-event bin. After data quality considerations, this yielded 161 reference events and 19 test events for use in the step 1 waveform location technique with location accuracy limited to the binning interval.

Relocation with hypoDD using NCSN data from 25 Berkeley network stations provided GT hypocenter information for the test events. We explored 4 different parameter settings controlling the extent of clustering and residual outlier rejection. Average standard deviations of GT locations for the 19 test events indicate good control on latitude and longitude (±0.015° and ±0.02°) and moderate control on depth (±1.23 km). We chose GT solutions with a mean errors (absolute value) of 0.03°, 0.04°, and 1.26 km.

In the step 1 procedure, the entire seismogram was filtered and an eigenvector decomposition of the covariance matrix was applied to the 3-component data (Rowe et al., 2002) prior to the calculation of Hilbert-envelopes for the principal direction. Test event data for each of the master stations were cross-correlated against 161 GT events with the position of the CC global maximum determining the step 1 location (Fig. 3). The Step 1 procedure located 14 of 19 test events to within 20 km (approximately 1 bin) of the NCSN catalog location with location error for the remaining events ranging from 25-50 km. Errors in test-event depth were < 1.5 km (1 depth bin) for half of the events and on the order of 2.5-10 km for the remaining step 1 relocated events.

The step 2 procedure attempts to improve upon the step 1 epicentral and depth estimates based on the use of catalog and WCC differential times with hypoDD. For each test event, subsets of the catalog and WCC data are prepared for use in hypoDD with the step 1 location providing the initial test-event location.

We augmented the existing P and S picks from the network catalog using skew and kurtosis analysis followed by a manual evaluation. Many catalog P picks required manual adjustment. We then prepared WCC data based on 3- and 5-second P windows (Rowe et al., 2002). A subset of non-test event data (P and S NCSN phase catalog times and WCC P-pick adjustments) augmented with test event data allows clustering of the test event with adjacent reference events. Clustering parameters for hypoDD are chosen to improve vertical control by strongly weighting pick data from event pairs with larger separation distances and WCC data from event pairs with smaller separation distances (Waldhauser, 2001).

We evaluated various ways of constructing pick and WCC data subsets. Relocation results were not influenced by the choice of distance cutoff in the cluster analysis. We used a cutoff value of 1° (reference event to test event) in our construction of pick and WCC data subsets. Construction of WCC differential time data subsets also depended on quality information, absolute arrival-time difference cutoff (5-15 s) and the minimum CC value (0.7-0.9). Both arrival-time and WCC data were influenced by choice of clustering parameters.

We also experimented with use of bispectrum-correlation (BC) values to validate WCC information with low CC values. An event was eligible for BC analysis if a station CC value was greater than a threshold value cutoff. Data from a subset of stations per event were selected for BC calculation based on a minimum CC value cutoff. If the BC and CC lag values were within a time-difference tolerance (0.25 s), BC data was allowed into the DD data set. The lowering of threshold value cutoffs (0.5-0.7) increased inclusion of BC data from 10% to 20% and led to a slight improvement in step 2 depth estimation over use of P pick WCC data with standard parameters (0.7 CC cutoff and maximum travel-time difference of 10 sec). Although we have not at this point adjusted catalog S picks, S-pick WCC data based on 30-s windowing were added to the P-pick WCC data as a final effort to improve depth estimation.

To test the stability of the step 2 procedure, locations were calculated using a range of starting depths (1.0, 2.5, 5.0, 10.0, 15.0, and 20.0 km) for each test event. Location mean and standard deviation values (Fig. 4) show that depths are less constrained for events outside of the ring of master stations, in particular the test events positioned near 34.3°. This is indicated by the tendency of the mean locations to shift towards the center of the test depth range and by larger depth standard deviations. Average standard deviation values of latitude, longitude, and depth for test events near 34.3° are larger (0.027°, 0.019°, 4.6 km) than within station coverage (0.004°, 0.013°, and 2.35 km) suggesting tradeoff in latitude and depth for the outside events. We attempted to improve the stability of the outlier events by adjusting WCC P-window length, including BC data, and adjusting parameters that control the use of WCC and BC data. A 5-second P window with a 0.9 cross-correlation cutoff was used to produce the results shown in Figure 4. The use of the BC data or other WCC parameter settings yields similar results.

We included S-wave WCC data to calculate step 2 relocations displayed in Figure 5, as it slightly lowered relocation errors for some of the events outside station coverage (34.3° latitude). The hypoDD relocation improves both epicenter and depth estimates (Fig. 5) both in resolution (GT error < bin intervals) and in accuracy. Seventeen of 19 test events have hypocenter location errors < 15 km, with 11 events relocated to within 5 km of GT. Depth errors for 16 events are within 2.5 km of GT. Mean latitude, longitude and depth errors (absolute value) for test events outside station coverage are larger (0.059°, 0.051°, and 2.5 km depth) by roughly a factor of 2 than mean errors within station coverage (0.028°, 0.031°, and 1.02 km depth). Step 2 location mean errors for events within station coverage are within the mean location error of the GT solution. Improvement of the S arrival-time picks over catalog times should lead to improved CC data and depth estimation. The accuracy of the relocation estimates even with coarse master station coverage suggests this approach could have broader application outside of this particular GT dataset study region.

Double-difference tomography

We have developed a new DD tomography method (Zhang and Thurber, 2003), which takes a step further of the DD location method (Waldhauser and Ellsworth, 2000) to solve for 3D velocity structure simultaneously with hypocenter locations using both catalog picks and differential arrival times (WCC and catalog). At the local scale (10s to 100s of kilometers), the earth can be represented with a flat model. We use the pseudo-bending ray-tracing algorithm (Um and Thurber, 1987) to find the rays and calculate the travel times between events and stations. The model is represented as a regular set of 3D nodes and the velocity values are interpolated by using the tri-linear interpolation method. The hypocentrer partial derivatives are calculated from the direction of the ray and the local velocity at the source. The ray path is divided into a set of segments and the model partial derivatives (calculated in terms of fractional slowness perturbation, so that the derivatives are related to path length) are evaluated by apportioning the derivative to its 8 surrounding nodes according to their interpolation weights on the segment midpoint (Thurber, 1983).

We have tested the local-scale version of DD tomography (tomoDD) with a synthetic dataset that was constructed on the basis of an idealized model of the velocity structure of the San Andreas Fault in central California (Kissling et al., 1994) shown in Figure 6. The events and stations used to construct the synthetic dataset are from the actual seismicity and USGS stations in the Loma Prieta region (Fig. 7). We added Gaussian random noise with zero mean and a standard deviation of 0.04 s to all the true arrival times. In addition, we also added a constant noise term to the arrivals at each station from a uniform distribution between –0.3 s and 0.3 s. This simulates the case that the systematic errors (model errors and pick bias) associated with the arrival times are larger than the random ones. We construct the pseudo "cross-correlation" data directly from the absolute arrival times by differencing the synthetic arrival times at common stations for events pairs within 20 km. As a result, the "cross-correlation" data are more accurate than the absolute data.

We first use the DD location algorithm *hypoDD* to relocate the events (Waldhauser, 2001). The 1D velocity model used is the Dietz and Ellsworth (1990) model, based on seismic refraction and earthquake data. We use both the residual weighting and distance weighting schemes in the inversion to control the large residuals, as did Waldhauser and Ellsworth (2000). The absolute differences between this set of event relocations and the true locations and their standard deviations are shown in Table 1. The results indicate that the event relocations from the DD location algorithm based on a 1D velocity model have a substantial bias (>1 km in each coordinate direction) from the true locations. This bias is caused by a difference between the velocity model (horizontal layers) used to calculate the DD locations and the true velocity model (vertical "sandwich") used to generate the data. The heterogeneity of the true velocity model makes path anomalies different for different events. However, the DD location method assumes that the path anomalies are location-independent, and this assumption introduces bias into event locations (Wolfe, 2002).

Next, we show the results of applying the standard tomography method to the relatively noisy absolute arrival times. The inversion starts from the same 1D velocity model as the DD location method. The X-Y nodes used to represent the velocity model are shown in Figure 7; in depth, nodes are positioned at 0, 3, 7, 11, and 16 km. The computational algorithm is identical to that for DD tomography, but the differential times are excluded. Both damping and smoothing (with weight 5.0 in both the horizontal and vertical directions) are applied to the inversion to make the solution more stable. Figure 8a shows horizontal slices through the velocity structure obtained from the standard tomography. The absolute difference between this velocity model and the true velocity model has a median value of 0.164 km/s, a mean value of 0.245 km/s and a standard deviation of 0.249 km/s. The main features of the true velocity model are evident in the depth slices. The event locations have smaller errors than those from the DD location method (Table 1).

DD tomography uses both the noisy absolute arrival times and more accurate differential times. We also apply damping and the smoothing constraints to stabilize the solution, with the residual weighting used to penalize the large residuals during the inversion. DD tomography starts with the same 1D velocity model and uses the same inversion grid as the standard tomography. Figure 8b shows the horizontal slices of the velocity structure from DD tomography. The absolute difference between this velocity structure and the true velocity structure has a median value of 0.136 km/s, a mean value of 0.178 km/s, and a standard deviation of 0.164 km/s. DD tomography characterizes well the low velocity zone of the true velocity model, especially at the depths of 3 km and 7 km. Subtracting the DD tomography solution and the standard tomography solution from the true model (Fig. 8c and d), we find that the velocity model from DD tomography has a more correct value in the low-velocity trough except at the depth of 0 km, where the ray paths from event pairs almost completely overlap and the accuracy of velocity

structure is mainly controlled by absolute catalog data. This indicates that DD tomography recovers better the low-velocity zone, and overall the velocity model is more accurate than the standard tomography. Compared with the standard tomography method, DD tomography also produces more accurate event locations (Table 1).

At the regional scale (100's to 1000's of km), however, the earth should not be treated as flat, but as a sphere. Some velocity discontinuities such as Conrad, Moho, and subducting slab boundary should also be taken into account. Finite-difference ray tracing algorithms developed by both Podvin and Lecomte (1991) and Hole and Zelt (1995) are able to accurately calculate first-arrival times in the presence of extremely severe, arbitrarily shaped velocity discontinuities. These algorithms solve a finite difference approximation to the Eikonal equation in the regularly gridded velocity structure through a systematic application of Huygens' principle. This procedure can explicitly take into account different propagation modes including transmitted and diffracted body waves, and head waves in addition to direct waves. The principle of reciprocity is utilized by placing the source point at the seismic station location and interpolating the travel times computed at the grid nodes to match the exact earthquake location (Flanagan et al., 1999).

To adapt the finite-difference algorithm to the regional scale, the curvature of the Earth must be taken into account. Earth flattening transformation is only valid for 1D velocity models and not for 3D velocity models. Following Flanagan et al. (2000), we solved this problem by parameterizing a spherical surface inside the Cartesian volume of grid nodes. The coordinate center was put at the surface of the Earth, positive X and Y-axes point to the direction of North and West, and positive Z-axis points downward, respectively. The grid nodes above the Earth surface (air nodes) are attributed to the true velocity values traveling in the air. As a result, all the rays travel inside the Earth. The regular uniform velocity (slowness) grid nodes used to calculate the travel time field using finite-difference algorithms are interpolated from the non-uniform inversion grid nodes through tri-linear interpolation. If an inversion grid node is 2 km above the Earth's surface, then it is treated as an air node and its value is fixed during the inversion. We treat each station as a source and calculate travel times to all velocity nodes in the volume. The travel time from a station to each earthquake is interpolated from its 8 neighboring nodes through tri-linear interpolation. The ray path from the earthquake to the station is found iteratively with increments opposite to the travel time gradient. After these setups, DD tomography is adapted to the regional scale with ray paths and related partial derivatives calculated by the finite-difference method. We have tested the regional-scale version of DD tomography on data from the subduction zone beneath northern Honshu, Japan, and obtained the velocity structure with unprecedented resolution.

CONCLUSIONS AND RECOMMENDATIONS

(1) WCC is vulnerable to problems associated with correlated noise that can be overcome using bispectrum analysis. It is our recommendation that a verification approach comparable to that described here be adopted for earthquake location applications for which very high accuracy is essential.

(2) A hierarchical location approach, for "new" events relative to a set of reference events, that starts with CC of long records at low frequencies to identify the approximate source region based solely on waveform similarity and then switches to DD location using CC of short records at high frequencies works effectively for a regional dataset from California. This approach should next be tested in a real-time monitoring environment.

(3) Algorithms for DD tomography have been successfully developed for both local (10's to a few 100 km) and regional (100's to 1000's of km) scale. Synthetic tests show the method yields locations with greater accuracy than either DD location or standard tomography, and a velocity model that is closer to the true model than standard tomography. The DD tomography approach works with either waveform-based or catalog-based differential time data, and thus is applicable to any dataset to which standard tomography can be applied.

ACKNOWLEDGEMENTS

We thank Megan Flanagan for providing codes for the spherical earth finite-difference method.

REFERENCES

Dodge, D. A., G. C. Beroza, and W. L. Ellsworth (1995), Foreshock sequence of the 1992 Landers, California, earthquake and its implications for earthquake nucleation, *J. Geophys. Res.*, 100, 9865-9880.

Flanagan, M. P., S. C. Myers, C. A. Schultz, M. E. Pasyanos, and J.Bhattacharyya (2000), Three-dimensional a priori model constraints and uncertainties for improving seismic location, 22nd Seismic Research Symposium: Technologies for Monitoring the CTBT, New Orleans, LA, *UCRL-JC-138984*.

Flanagan, M.P., C. A. Schultz, and L. J. Hutchings (1999), Development of 3-D crust and upper mantle velocity models to improve seismic event location, AGU Fall meeting, San Francisco, CA, *EOS Trans. Am. Geophys. Un.*, 80, p. F656.

Got, J.-L., J. Fréchet, and F. W. Klein (1994), Deep fault plane geometry inferred from multiple relative relocation beneath the south flank of Kilauea, *J. Geophys. Res.*, 99, 15,375-15,386.

Hole, J. A., and B. C. Zelt (1995), 3-D finite-difference reflection traveltimes, *Geophys. J. Int.*, 121, 427-434.

Kissling, E., W. L. Ellsworth, D. Eberhart-Phillips, and U. Kradolfer (1994), Initial reference models in local earthquake tomography, *J. Geophy. Res.*, 99, 19.635-19,646.

Nikias, C. L., and M. R. Raghuveer (1987), Bispectrum estimation: A digital signal processing framework, *Proc. IEEE*, 75, 869-891.

Nikias, C. L., and R. Pan (1988), Time delay estimation in unknown Gaussian spatially correlated noise, *IEEE Trans. Acoust. Speech Signal Processing*, 36, 1706-1714.

Podvin, P., and I. Lecomte (1991), Finite difference computation of travel times in very contrasted velocity models: a massively parallel approach and its associated tools, *Geophys. J. Int.*, 105, 271-284.

Poupinet, G., W. L. Ellsworth, and J. Fréchet (1984), Monitoring velocity variations in the crust using earthquake doublets: an application to the Calaveras fault, California, *J. Geophys. Res.*, 89, 5719-5731.

Rowe, C.A., R.C. Aster, B. Borchers and C.J. Young (2002), An automatic, adaptive algorithm for refining phase picks in large seismic data sets, *Bull. Seismol. Soc. Am.*, 92, 1660.

Rubin, A. M., D. Gillard, and J.-L. Got, Streaks of microearthquakes along creeping faults (1999), *Nature*, 400, 635-641.

Schaff, D. P., G. H. R. Bokelmann, G. C. Beroza, F. Waldhauser, and W. L. Ellsworth (2002), High-resolution image of Calaveras Fault seismicity, *J. Geophys. Res.*, 107, 2186, doi:10.1029/2001JB000633.

Shearer, P. M. (1997), Improving local earthquake locations using the L1 norm and waveform cross correlation: Application to the Whittier Narrows, California, aftershock sequence, *J. Geophys. Res.*, 102, 8269-8283.

Thurber, C. H. (1983), Earthquake locations and three-dimensional crustal structure in the Coyote Lake area, central California, *J. Geophys. Res.*, 88, 8226-8236.

Um, J., and C. H. Thurber (1987), A fast algorithm for two-point seismic ray tracing, *Bull. Seism. Soc. Am.*, 77, 972-986.

Waldhauser, F. (2001), hypoDD: A computer program to compute double-difference hypocenter locations, *U.S. Geol. Surv. Open File Rep.*, 01-113, 25 pp.

Waldhauser, F., and W.L. Ellsworth (2000), A double-difference earthquake location algorithm: Method and application to the Northern Hayward Fault, California, *Bull. Seism. Soc. Am.*, 90, 1353-1368.

Wolfe, C. J. (2003), On the mathematics of using difference operators to relocate earthquakes, *Bull. Seism. Soc. Am.*, 92, 2879-2892.

Yung, S. K., and L. T. Ikelle (1997), An example of seismic time picking by third-order bicoherence, *Geophys.*, 62, 1947-1951.

Zhang, H., and C. H. Thurber (2003), Double-difference tomography: The method and its application to the Hayward fault, California, *Bull. Seism. Soc. Am.*, in press.

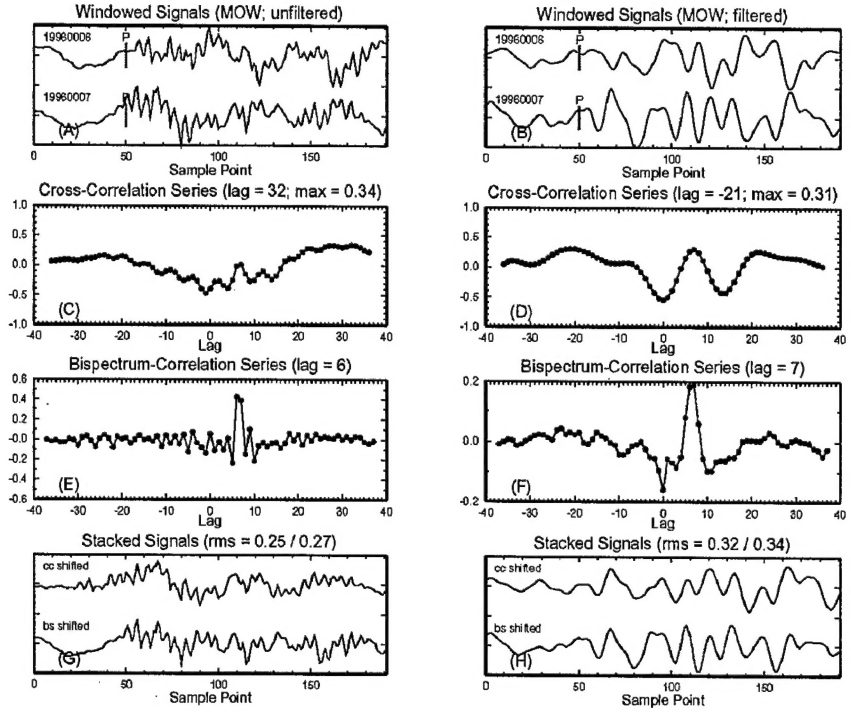

Figure 1. (A) Windowed waveforms (1 second before and 2.82 seconds after the catalog P pick) for two New Zealand earthquakes recorded at station MOW. The station sampling rate is 50 sample/sec and the signals are aligned by the P picks. (B) Windowed waveforms band-pass filtered between 1 and 6 Hz. (C, D) CC series for the (C) unfiltered (raw) and (D) filtered waveforms. (E,F) Bispectrum-correlation series for the(E) raw and (F) filtered waveforms. (G) Stacked raw waveforms. The upper trace is obtained by shifting the waveform of the first event with the CC determined lag relative to the second one, while the lower trace is computed after shifting the waveform of the first event with the lag calculated with the bispectrum method. The root-mean-square amplitudes for the two traces are 0.25 and 0.27 respectively. (H) Same as G for the stacked band-pass filtered waveforms. The root-mean-square amplitudes for the two traces are 0.32 and 0.34 respectively.

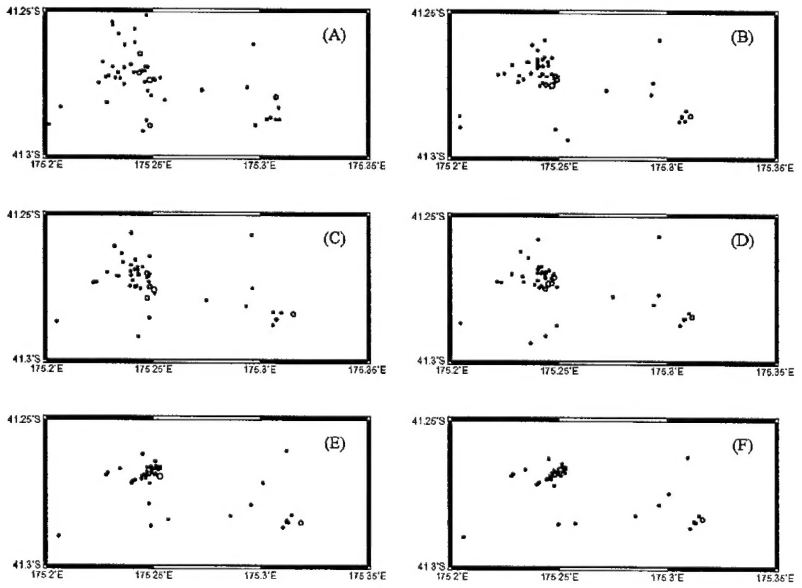

Figure 2. Locations of 53 earthquakes near lake Wairarapa, NZ. (A) Before relocation; (B) relocated with catalog differential travel times; (C) relocated with CC differential travel times chosen with the threshold criterion; (D) relocated with CC differential travel times verified with the bispectrum method; (E) relocated with both catalog and threshold-chosen CC differential travel times; (F) relocated with both catalog and bispectrum-verified CC differential travel times.

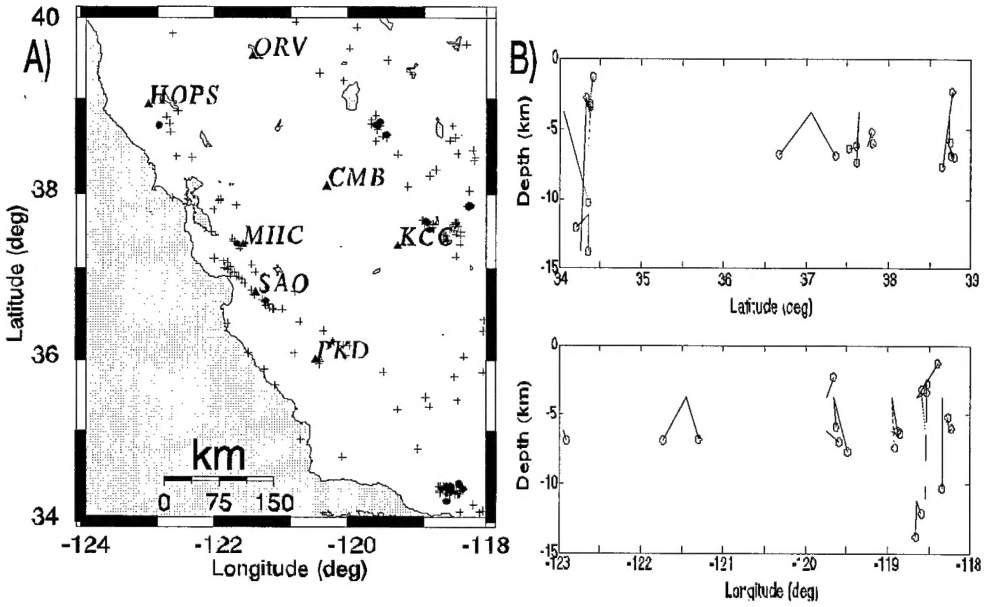

Figure 3. A) Map of study region showing the 7 master stations used in the step 1 procedure, 161 reference events, and 19 test events. Stations are indicated by triangles and labeled by their BK network station abbreviation. Test and reference events are indicated by '*' and '+' symbols respectively. Usage of hypoDD to construct GT for test events and in the step 2 relocation includes catalog data from 18 Berkeley network stations in addition to the 7 master stations for a total station range of .35.9° to 41.9° latitude and –119.3° to –124.07° longitude. B) Step 1 derived mislocation of hypocenter indicated by lines connecting the step 1 location with the hypoDD based GT location ('o' symbol). Events positioned outside master station coverage (near 34° latitude) have larger mislocation errors relative to GT than test events within the circumference of master station coverage.

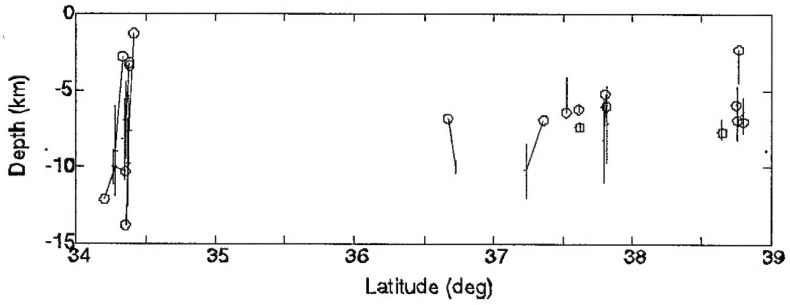

Figure 4. Stability test showing poorer depth constraint for events outside the set of master stations. The mislocation is indicated by solid line connecting the mean step 2 location with the hypoDD GT location ('o' symbol). The vertical and horizontal lines at the mean step 2 location indicate standard deviations of the step 2 estimates of depth and latitude.

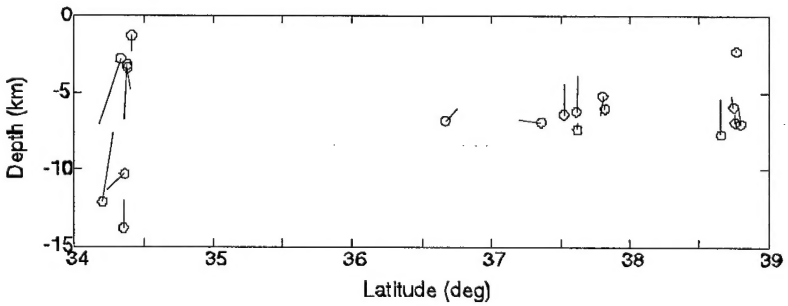

Figure 5. Step 2 mislocation of hypocenters indicated by lines connecting the step 2 location with the hypoDD based GT location ('o' symbol).

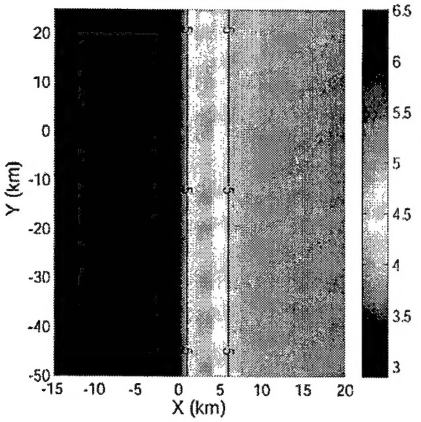

Figure 6. A horizontal slice through the true synthetic velocity model. The true velocity model in 3D is similar to a "vertical sandwich," with velocity constant with depth.

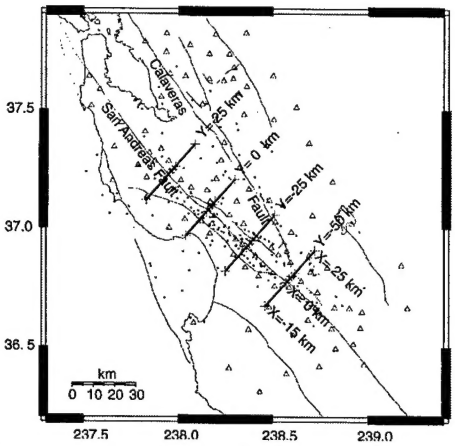

Figure 7. Event locations (filled circles) and stations (triangles) used for the synthetic data set. The inversion grid used in the standard and DD tomography solutions is shown as crosses. The inversion grid points are at X=-35, -15, 0, 2, 4, 6, 20, 35 km, at Y=-60, -40 –20, 0, 20, 40 km, and at Z=0, 3, 7, 11, 16 km.

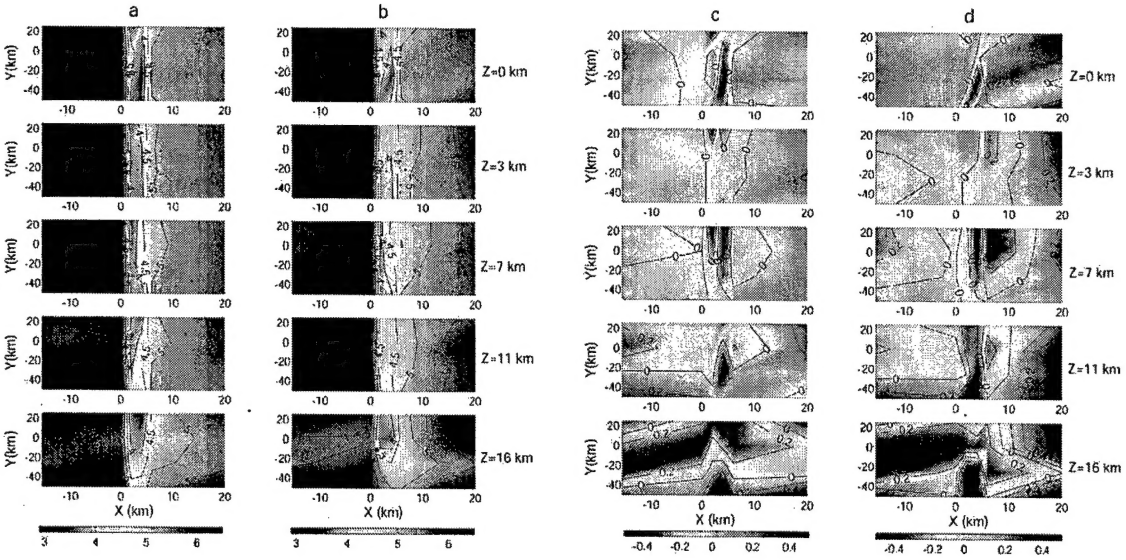

Figure 8. Horizontal slices through the velocity models from (a) standard tomography and (b) DD tomography, and the difference between (c) the DD tomography solution and the true model and (d) the standard tomography solution and the true model. Black dots indicate the earthquake hypocenters within half the grid-size of the slice.

Table 1. The absolute differences between the true locations and those from the DD location method based on 1D velocity model, standard tomography, and DD tomography.

	Median value (km)			Standard deviation (km)		
	Latitude	Longitude	Depth	Latitude	Longitude	Depth
DD location (1D)	1.131	1.235	1.123	0.976	0.941	1.658
Standard tomography	0.320	0.295	0.460	0.399	0.342	0.575
DD tomography	0.238	0.218	0.329	0.288	0.314	0.427